


Nonlinear analysis of a 2-DOF piecewise linear aeroelastic system

Tamás Kalmár-Nagy · Rudolf Csikja  · Tarek A. Elgohary

Received: 1 December 2015 / Accepted: 2 March 2016
© Springer Science+Business Media Dordrecht 2016

Abstract We study the dynamics of a two-degree-of-freedom (pitch and plunge) aeroelastic system where the aerodynamic forces are modeled as a piecewise linear function of the effective angle of attack. Stability and bifurcations of equilibria are analyzed. We find border collision and rapid bifurcations. Bifurcation diagrams of the system were calculated utilizing MATCONT and *Mathematica*. Chaotic behavior with intermittent switches about the two nontrivial equilibria was also observed.

Keywords Aeroelasticity · Piecewise linear system · Limit cycle oscillation · Bifurcation · Hybrid system · Chaos

1 Introduction

Nonlinear analysis of airfoils is a topic that is extensively covered in the literature [7, 11, 12, 18]. In general, nonlinearities of airfoils are structural and/or aerodynamic. A comprehensive analysis for such nonlinearities was presented in [18] together with the derivation of the equations of motion of a 2D airfoil oscillating in pitch and plunge. The authors investigated stability, bifurcations and chaos of the system with cubic, freeplay and hysteresis. Nonlinear aeroelasticity and its effects on flight and its association with limit cycle oscillations (LCO's) was considered in [7]. Gilliat et al. [11] studied both structural and aerodynamic nonlinearities arising from stall conditions.

An experimental investigation of structural nonlinearity with emphasis given to continuous nonlinearities arising from spring hardening/softening effects was presented in [25] and [26]. The aeroelastic response of a 2D airfoil with bilinear and cubic structural nonlinearities was investigated in [29]. Numerical simulations applying the finite difference method were compared against the analytical describing function method. LCO's were found to exist at a velocity below the divergent flutter limit. Chaotic behavior was investigated with the application of preload, and bifurcation diagrams showing period doubling were plotted as a result. Similarly, freeplay, hysteresis and cubic structural nonlinearities were analyzed in [39]. The flutter behavior of the airfoil was found to be highly depen-

T. Kalmár-Nagy
Department of Fluid Mechanics, Faculty of Mechanical Engineering, Budapest University of Technology and Economics, Budapest, Hungary
e-mail: nd@kalmarnagy.com

R. Csikja (✉)
Mathematics Institute, Faculty of Natural Sciences, Budapest University of Technology and Economics, Budapest, Hungary
e-mail: csikja@math.bme.hu

T. A. Elgohary
Aerospace Engineering Department, Texas A&M University, College Station, USA
e-mail: tarek168@tamu.edu

dent on initial conditions. LCO's existence arising from those nonlinearities was also investigated. Abdelkefi et al. [1] perform an analytical and experimental investigation into the dynamics of an aeroelastic system consisting of a plunging and pitching rigid airfoil supported by a linear spring in the plunge degree of freedom (DOF) and a nonlinear spring in the pitch DOF.

Aerodynamic nonlinearities were investigated separately in [37]. A typical airfoil section with transonic aerodynamic nonlinearities was analyzed using the describing function method. Results compared to numerical methods were found to be very close especially for small amplitudes of motion where the describing function method is very effective. Internal resonances in a 2D airfoil model with aerodynamic nonlinearities arising from dynamic stall were examined in [12]. The existence of internal resonances in specific classes of aeroelastic systems was investigated which lead to instabilities that were not predicted by traditional methods.

Combining both structural and aerodynamic nonlinearities was investigated in the aeroelastic response of a nonrotating helicopter blade in [34] and [35]. The airfoil model was a NACA 0012 with three cases of nonlinearities, nonlinear structure linear aerodynamics, linear structure nonlinear aerodynamics and nonlinear structure with nonlinear aerodynamics, analyzed numerically. Structural nonlinearities were modeled by freeplay stiffness, whereas experimental data and curve fitting techniques were used to model the nonlinear aerodynamic lift coefficient. The flutter behavior in all cases was investigated, and the amplitudes of LCO's were found to be dependent on freestream velocity and initial conditions. Chaotic behavior was also investigated for forced and unforced cases with Poincaré maps for certain velocities. Experimental and analytical results were found to be in good agreement. Freeplay, cubic and hysteresis structural nonlinearities were also investigated on 2-DOF and 3-DOF models. The analysis confirmed that the flutter amplitudes were largely dependent on initial conditions.

Representing a nonlinear continuous system as piecewise linear is generally used to make the problem more tractable. This approach was used in [3] for several problems involving forced and free oscillations. Hysteretic systems are also analyzed using this method [16], where a hysteretic relay oscillator was analyzed, explicit solution of the problem was found and Poincaré maps of the system were constructed. In [27] and [28],

the same approach was used to describe the behavior of an elasto-plastic beam model. The authors showed the hysteretic behavior of the system after finding the closed-form solution of the problem and constructing a map for the determination of the plastic cycles of the system. The problem was tackled with both free and periodic impulse forcing oscillations. A piecewise linear oscillation model was utilized in [32] to analyze a single-DOF nonlinear oscillator with nonlinearity in the restoring force. The force was modeled as a piecewise linear function with a single change of slope. Poincaré maps of the system was also analyzed, and harmonic, subharmonic and chaotic motions were found with the bifurcations leading to them. Similarly, in [22] and [23], two types of piecewise linear systems were introduced and analyzed: systems with setup springs and systems with clearances. Subharmonic and chaotic motions of those systems were also investigated and analyzed. Bifurcations in nonsmooth continuous systems are discussed in [5, 19], and a recent survey of the field can be found in [24]. The so-called multiple crossing bifurcations where the eigenvalues jump more than once over the imaginary axis were discussed for those types of systems with several examples of systems with that type of bifurcation. Magri and Galvanetto [21] shows how the nonsmooth definition of the dynamic stall model can generate a nonsmooth Hopf bifurcation in an aeroelastic system. Antali and Stepan [4] explore discontinuity-induced bifurcations for a ball in dual-point contact with a cylindrical vessel. Llibre et al. [20] deal with determining the maximum number of limit cycles of some classes of planar discontinuous piecewise linear differential systems defined in two half-planes separated by a straight line.

In this work, a 2-DOF (pitch and plunge) aeroelastic system is analyzed with a piecewise linear aerodynamic model. First, the piecewise aerodynamic model is described and the range of each portion of the model is defined. The equations of motion are then derived and expressed in terms of the piecewise linear model parameters and then nondimensionalized. From the piecewise linear model, a bilinear model is extracted for the analysis. The stability and bifurcations of the bilinear system are examined analytically and numerically. The analysis found bifurcations that are intrinsic to piecewise systems such as border collision and the rapid bifurcations. The border collision bifurcation describes the sudden birth of equilibria, and the rapid bifurcation explains the creation of a finite-amplitude stable

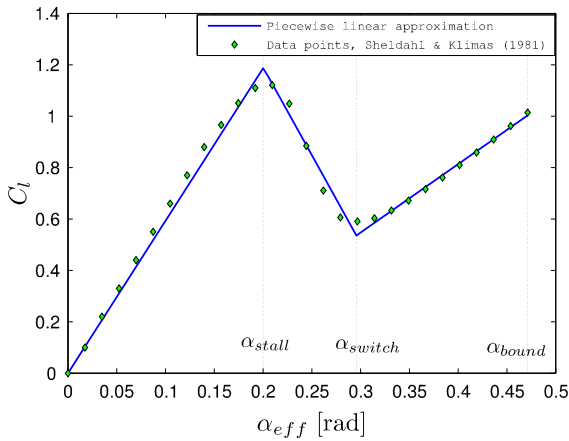


Fig. 1 Experimental lift coefficient data and piecewise linear approximation

limit cycle. Chaotic behavior was also found, and the intermittent route to chaos was observed numerically. We comment on the validity of the bilinear model and examine the robustness of the solutions by introducing a family of function to provide a smooth transition between the pre-stall and post-stall regimes.

2 The aeroelastic system

2.1 Aerodynamic forces

A comprehensive experimental study of lift coefficient versus angle of attack was presented in [33]. Data were collected for seven airfoil sections, all looking similar to the NACA 0012 data shown in Fig. 1.

Motivated by the appearance of the data, the lift coefficient C_l is modeled as a piecewise linear function of the effective angle of attack α_{eff} (note that C_l is an odd function of α_{eff}). The piecewise linear model consists of three portions with boundaries defined by α_{stall} , α_{switch} and α_{bound} , as shown in Fig. 1. The parameter α_{stall} characterizes the stall condition at which lift starts to decrease as α_{eff} is increased. The parameter α_{switch} corresponds to the switching point at which the slope of C_l starts to increase again. The parameter α_{bound} defines the range of validity of the model. The lift coefficient $C_l(\alpha_{eff})$ is therefore defined as

$$C_l(\alpha_{eff}) = \begin{cases} c_0\alpha_{eff} & |\alpha_{eff}| \leq \alpha_{stall} \\ c_1\alpha_{eff} + \text{sgn}(\alpha_{eff})c_2 & \alpha_{stall} \leq |\alpha_{eff}| \leq \alpha_{switch} \\ c_3\alpha_{eff} + \text{sgn}(\alpha_{eff})c_4 & \alpha_{switch} \leq |\alpha_{eff}| \leq \alpha_{bound}. \end{cases} \quad (1)$$

Table 1 Piecewise linear aerodynamic model parameters

c_0	c_1	c_2	c_3	c_4
5.932	-6.846	2.56	2.662	-0.2515
α_{stall}	α_{switch}	α_{bound}		
0.2 rad	0.2957 rad	0.4712 rad		

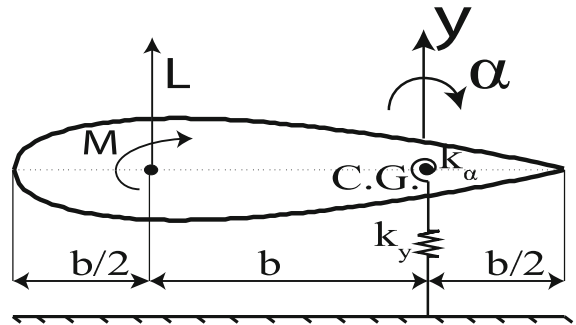


Fig. 2 2-DOF pitch and plunge model

The parameters (summarized in Table 1) are found by manual partitioning of the data followed by least square line fitting. A more rigorous way of fitting a continuous, piecewise linear function to data is described in [38].

2.2 Dynamic model

The dynamic model is a typical 2-DOF, pitch and plunge, aeroelastic system shown in Fig. 2. The variable y describes the vertical (plunge) displacement, α is the angular (pitch) displacement, k_y is the linear spring constant for the plunge DOF, k_α is the torsional spring constant for the pitch DOF, M , L are the aerodynamic moment and lift applied at the airfoil aerodynamic center, and finally, b is the semichord of the airfoil. A simplifying assumption we use is that the aeroelastic axis and the center of mass are collocated at three quarters of the chord length.

The system equations are given by

$$m\ddot{y} + c_y\dot{y} + k_y y = -L(C_l(\alpha_{eff})), \quad (2)$$

$$I_{cg}\ddot{\alpha} + c_\alpha\dot{\alpha} + k_\alpha\alpha = M(C_l(\alpha_{eff})), \quad (3)$$

where m is the mass of the wing, c_y is the damping coefficient for the plunge DOF, I_{cg} is the moment of inertia about the center of mass and c_α is the damping coefficient for the pitch DOF. The effective angle of

Table 2 System parameters

Parameter	Description	Value/units
b	Semichord of wing	0.1064 m
S	Wing span	0.6 m
m	System mass	12 kg
k_y	Spring constant plunge DOF	2844.4 N/m
k_α	Spring constant pitch DOF	2.82 N m/rad
c_y	Viscous damping plunge DOF	27.43 kg/s
c_α	Viscous damping pitch DOF	0.036 kg m ² /s
I_{cg}	Mass moment of inertia	0.0433 kg m ²
ρ	Air density	1.2 kg/m ³
L	Aerodynamic lift	N
M	Aerodynamic moment	N m
y	Plunge DOF	m
α	Pitch DOF	rad
U	Freestream velocity	m/s

attack α_{eff} takes into account the instantaneous motion of the system and is defined as

$$\alpha_{\text{eff}} = \alpha + \frac{\dot{y}}{U}, \tag{4}$$

where U is the freestream velocity. The aerodynamic lift and moment as functions of the lift coefficient are given by

$$L(C_l(\alpha_{\text{eff}})) = \rho U^2 b S C_l(\alpha_{\text{eff}}), \tag{5}$$

$$M(C_l(\alpha_{\text{eff}})) = \rho U^2 b^2 S C_l(\alpha_{\text{eff}}). \tag{6}$$

Here ρ is the air density and S is the wing span. Table 2 summarizes the system parameters together with their values used in our computations (from [33]).

2.3 Nondimensional model

Equations (2)–(6) are nondimensionalized by a length scale L , a time scale T , and a nondimensional freestream velocity $\mu > 0$, given by

$$L^2 = \frac{I_{cg}}{\rho b^2 S}, \quad T^2 = \frac{m}{k_y}, \quad \mu = \frac{U}{L/T}. \tag{7}$$

These scales yield the nondimensional plunge, $\tilde{y} = \frac{y}{L}$, the nondimensional time $\tau = \frac{t}{T}$. The derivative with respect to the nondimensional time is denoted by $(\prime) =$

$\frac{d(\cdot)}{d\tau}$. The nondimensional angle of attack can now be expressed as

$$\alpha_{\text{eff}} = \alpha + \frac{1}{\mu} \tilde{y}'. \tag{8}$$

By substituting the piecewise linear function C_l into the Eqs. (2) and (3), we get

$$\begin{aligned} \tilde{y}'' + p_1 \tilde{y}' + \tilde{y} &= -p_2 \mu^2 C_l(\alpha_{\text{eff}}), \\ \alpha'' + p_3 \alpha' + p_4 \alpha &= \mu^2 C_l(\alpha_{\text{eff}}), \end{aligned} \tag{9}$$

with which we obtain the equations for $-\alpha_{\text{stall}} \leq \alpha_{\text{eff}} \leq \alpha_{\text{stall}}$

$$\begin{aligned} \tilde{y}'' + (p_1 + p_2 \mu c_0) \tilde{y}' + \tilde{y} + p_2 \mu^2 c_0 \alpha &= 0, \\ \alpha'' + p_3 \alpha' + (p_4 - \mu^2 c_0) \alpha - \mu c_0 \tilde{y}' &= 0, \end{aligned} \tag{10}$$

for $\alpha_{\text{stall}} \leq |\alpha_{\text{eff}}| \leq \alpha_{\text{switch}}$

$$\begin{aligned} \tilde{y}'' + (p_1 + p_2 \mu c_1) \tilde{y}' + \tilde{y} + p_2 \mu^2 c_1 \alpha &= \\ = -p_2 \mu^2 c_2 \text{sgn}(\alpha_{\text{eff}}) \alpha'' + p_3 \alpha' &+ \\ + (p_4 - \mu^2 c_1) \alpha - \mu c_1 \tilde{y}' = \mu^2 c_2 \text{sgn}(\alpha_{\text{eff}}), \end{aligned} \tag{11}$$

and for $\alpha_{\text{switch}} \leq |\alpha_{\text{eff}}| \leq \alpha_{\text{bound}}$

$$\begin{aligned} \tilde{y}'' + (p_1 + p_2 \mu c_3) \tilde{y}' + \tilde{y} + p_2 \mu^2 c_3 \alpha &= \\ = -p_2 \mu^2 c_4 \text{sgn}(\alpha_{\text{eff}}), & \\ \alpha'' + p_3 \alpha' + (p_4 - \mu^2 c_3) \alpha - \mu c_3 \tilde{y}'^2 c_4 \text{sgn}(\alpha_{\text{eff}}). \end{aligned}$$

The nondimensional parameters p_1, p_2, p_3 and p_4 are given by

$$\begin{aligned} p_1 &= \frac{c_y}{\sqrt{m k_y}}, & p_2 &= \frac{\sqrt{\rho I_{cg} S}}{m}, \\ p_3 &= \frac{c_\alpha}{I_{cg} \sqrt{k_y}}, & p_4 &= \frac{k_\alpha m}{I_{cg} k_y}. \end{aligned} \tag{12}$$

3 The bilinear model

Since a bilinear model is more tractable for the purpose of understanding the full system behavior, so here we restrict our attention to such a model. Further, using the bilinear model lets the aerodynamic model exceed the physical bounds of the original aeroelastic system resulting in a more general solution that can be applied to several classes of problems, see [9] and [17].

Figure 16 shows the full bilinear model and the odd nature of the lift coefficient function.

By introducing the new variables

$$x_1 := \tilde{y}, \quad x_2 := \tilde{y}', \quad x_3 := \alpha, \quad x_4 := \alpha' \tag{13}$$

and the state vector $\mathbf{x} := (x_1, x_2, x_3, x_4)^\top$, Eqs. (10)–(11) can be concisely written as the piecewise linear system

$$\dot{\mathbf{x}} = \mathbf{A}_1 \mathbf{x} - \mathbf{B}, \quad \mathbf{x} \in \Omega^- \cup \Sigma^-, \tag{14}$$

$$\dot{\mathbf{x}} = \mathbf{A}_0 \mathbf{x}, \quad \mathbf{x} \in \Sigma^- \cup \Omega^0 \cup \Sigma^+, \tag{15}$$

$$\dot{\mathbf{x}} = \mathbf{A}_1 \mathbf{x} + \mathbf{B}, \quad \mathbf{x} \in \Sigma^+ \cup \Omega^+. \tag{16}$$

Here

$$\mathbf{A}_k = \begin{pmatrix} 0 & 1 & 0 & 0 \\ -1 - c_k \mu p_2 - p_1 & -\mu^2 c_k p_2 & 0 & 0 \\ 0 & 0 & 0 & 1 \\ 0 & c_k \mu & c_k \mu^2 - p_4 & -p_3 \end{pmatrix},$$

$$\mathbf{B} = \begin{pmatrix} 0 \\ -c_2 p_2 \mu^2 \\ 0 \\ c_2 \mu^2 \end{pmatrix}$$

and all symbols but c_1 are positive, see (12) and Tables 1 and 2. The system has one parameter $\mu > 0$. The domains of the subsystems (14)–(16) are given by

$$\begin{aligned} \Omega^\pm &:= \left\{ \mathbf{x} \in \mathbb{R}^4 : \pm(x_3 + x_2/\mu) > \alpha_{\text{stall}} \right\}, \\ \Omega^0 &:= \left\{ \mathbf{x} \in \mathbb{R}^4 : |x_3 + x_2/\mu| < \alpha_{\text{stall}} \right\}. \end{aligned} \tag{17}$$

These domains are separated by the switching planes defined by

$$\Sigma^\pm := \left\{ \mathbf{x} \in \mathbb{R}^4 : x_3 + x_2/\mu = \pm \alpha_{\text{stall}} \right\}. \tag{18}$$

With these, the state space \mathbb{R}^4 can be decomposed as

$$\mathbb{R}^4 = \Omega^- \cup \Sigma^- \cup \Omega^0 \cup \Sigma^+ \cup \Omega^+.$$

This decomposition is demonstrated in Fig. 4.

3.1 Equilibria: existence, stability and bifurcations

In the following, we will show that the origin is always an equilibrium of the system, and depending on the

parameter value, there could be two other equilibria (\mathbf{E}^\pm). To ascertain the stability of these equilibria, we study the characteristic polynomial of \mathbf{A}_k

$$R_k = \lambda^4 + a_1(k, \mu)\lambda^3 + a_2(k, \mu)\lambda^2 + a_3(k, \mu)\lambda + a_4(k, \mu), \tag{19}$$

$$a_1(k, \mu) = p_3 + p_1 + p_2 c_k \mu, \tag{20}$$

$$a_2(k, \mu) = 1 + p_4 + p_1 p_3 + p_2 p_3 c_k \mu - c_k \mu^2, \tag{21}$$

$$a_3(k, \mu) = p_3 + p_1 p_4 + p_2 p_4 c_k \mu - p_1 c_k \mu^2, \tag{22}$$

$$a_4(k, \mu) = p_4 - \mu^2 c_k. \tag{23}$$

Applying the Liénard–Chipart stability criterion [10], the matrix \mathbf{A}_k is asymptotically stable if and only if

$$a_2(k, \mu) > 0, \tag{24}$$

$$a_4(k, \mu) > 0, \tag{25}$$

$$\Delta_1(k, \mu) = a_1(k, \mu) > 0, \tag{26}$$

$$\begin{aligned} \Delta_3(k, \mu) &= \mu^5 c_k^3 p_1 p_2 \\ &+ \mu^4 c_k^2 \left(p_1 p_3 - p_2^2 (p_1 p_3 + p_4 - 1) c_k \right) \\ &+ \mu^3 p_2 c_k^2 \left(p_3 \left(p_4 \left(p_2^2 c_k - 1 \right) + 1 \right) - 2 p_3 p_1^2 - \right. \\ &\quad \left. \times \left(p_3^2 + p_4 - 1 \right) p_1 \right) \\ &+ \mu^2 p_3 c_k \left(p_1 \left(p_4 \left(3 p_2^2 c_k - 2 \right) + 2 \right) \right. \\ &\quad \left. + p_2^2 p_3 (p_4 + 1) c_k - p_1^2 (p_1 + p_3) \right) \\ &+ \mu p_2 p_3 c_k \left(3 p_4 p_1^2 + 2 p_3 (p_4 + 1) p_1 \right. \\ &\quad \left. + p_3^2 + (p_4 - 1)^2 \right) \\ &+ p_1 p_3 \left(p_3^2 + (p_4 - 1)^2 + p_1^2 p_4 \right. \\ &\quad \left. + p_1 p_3 (p_4 + 1) \right) > 0, \end{aligned} \tag{27}$$

where Δ_1 and Δ_3 are the so-called Hurwitz determinants.

3.1.1 Stability of the origin

Subsystem (15) always admits the origin as equilibrium. Notice that the left-hand sides of (24)–(27) are all positive at $\mu = 0$; therefore, by continuity the origin is stable for small enough $\mu > 0$.

Figure 3 shows the behavior of the eigenvalues of \mathbf{A}_0 [subsystem (15)].

One complex conjugate pair (denoted by λ_A) moves very little and remains in the left half plane. As the

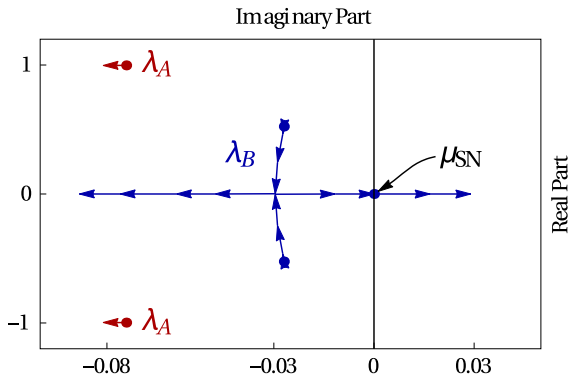


Fig. 3 Eigenvalues of A_0 as a function of μ

imaginary parts of the complex conjugate pair λ_B move toward zero, they collide and become real (this is a case of colliding eigenvalues [31]), still in the left half complex plane. This eigenvalue collision happens at $\mu_{EC} \approx 0.2149$.

Then this pair splits in dispair along the real axis. To see where the origin loses stability (when one real root moves to the right half plane), we need to find the smallest positive μ for which any of the inequalities (24)–(27) is violated. In other words, we are looking for the smallest positive root of any of $a_2(0, \mu) = 0$, $a_4(0, \mu) = 0$, $\Delta_1(0, \mu) = 0$, $\Delta_3(0, \mu) = 0$. Notice that $\Delta_1(0, \mu)$ and $\Delta_3(0, \mu)$ are always positive, since $\Delta_1(0, \mu) = p_3 + p_1 + p_2c_0\mu > 0$ and

$$\Delta_3(0, \mu) = 0.0044 + 0.0029\mu + 0.0676\mu^2 + 0.0746\mu^3 + 0.3145\mu^4 + 0.456\mu^5 > 0.$$

Therefore, $\Delta_1(0, \mu) = 0$ and $\Delta_3(0, \mu) = 0$ have no positive roots. Now, observe that

$$a_4(0, \mu) < a_2(0, \mu) = a_4(0, \mu) + c_0p_2p_3\mu + p_1p_3 + 1,$$

and both $a_2(0, \mu)$ and $a_4(0, \mu)$ are quadratic in μ with negative leading coefficients. Hence, $a_4(0, \mu) = 0$ has the smallest positive root given by

$$\mu_{SN} := \sqrt{\frac{p_4}{c_0}} \approx 0.2152. \tag{28}$$

The subscript SN is used because at this parameter value the origin undergoes a saddle–node bifurcation in the two-dimensional subspace corresponding to the eigenvalue pair λ_B (see Fig. 3).

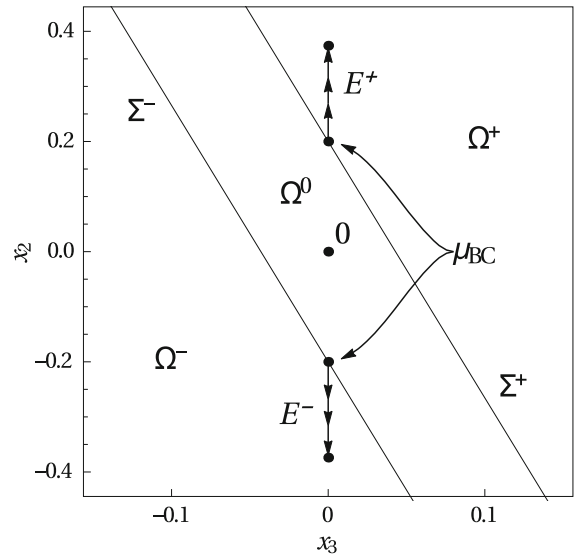


Fig. 4 The equilibria E^\pm as a function μ

3.1.2 Existence and stability of E^\pm

Subsystems (14), (16) have as equilibria

$$E^\pm = \mp A_1^{-1}B = \mp \frac{c_2\mu^2}{c_1\mu^2 - p_4} \begin{pmatrix} -p_2p_4 \\ 0 \\ 1 \\ 0 \end{pmatrix}, \tag{29}$$

when these are in the domain of subsystems (14), (16), respectively, i.e.,

$$\mu \geq \mu_{BC} := \sqrt{\frac{p_4\alpha_{stall}}{c_2 + c_1\alpha_{stall}}} \approx 0.2148. \tag{30}$$

This condition can be easily derived from the inclusion

$$E^\pm \in \Omega^\pm \cup \Sigma^\pm, \tag{31}$$

since the norms of the equilibria $\|E^\pm\|$ are monotonically increasing functions of μ (in other words E^\pm are points moving away from the origin on a line as μ is increased). At $\mu = \mu_{BC}$, the system undergoes a discontinuity-induced bifurcation, called border collision bifurcation [5,41]. The positions of the equilibria and the bifurcation are depicted in Fig. 4 together with the subsystem domains and the switching lines. Note that the switching lines are also dependent on μ , Fig. 4 only shows them for the bifurcation value $\mu = \mu_{BC}$.

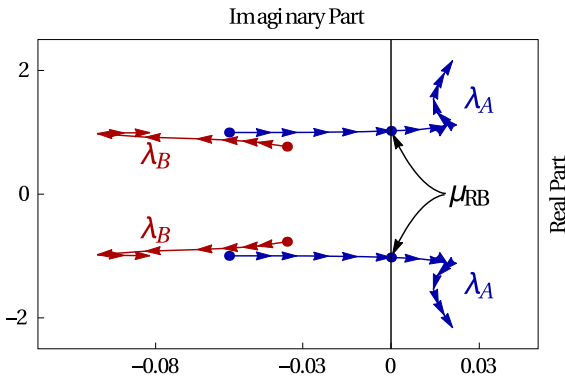


Fig. 5 Eigenvalues of A_1 as a function of μ

The equilibria E^\pm lose stability when the pair of conjugate roots λ_A of the characteristic polynomial $R_1 = 0$ crosses the imaginary axis (see Fig. 5). To find the parameter value μ_{RB} (the subscript refers to the rapid bifurcation created at this value; see next Section) where this occurs, again we need to find the smallest positive μ for which any of the inequalities (24)–(27) is violated. Except in this case, the polynomials contain $c_1 < 0$ instead of $c_0 > 0$ (i.e., $k = 1$). One can easily see that $0 < a_4(1, \mu)$, and the discriminant of $a_2(1, \mu)$ turns out to be negative; therefore, $a_2(1, \mu)$ and $a_4(1, \mu)$ have no positive real roots for $\mu > 0$. Now, examining the other two polynomials $\Delta_1(1, \mu)$ and $\Delta_3(1, \mu)$, we have the following results. The only root of $\Delta_1(1, \mu) = 0$ is $\mu \approx 2.01$, and the only positive root of $\Delta_3(1, \mu) = 0$ is $\mu \approx 0.3034$, which is the smaller one; hence, at $\mu_{RB} \approx 0.3034$ the equilibria E^\pm lose stability.

3.1.3 Bifurcation diagram

For $0 < \mu < \mu_{BC}$, the origin is the only equilibrium (stable). Then at $\mu = \mu_{BC}$ two equilibria E^\pm appear in symmetric positions on the switching planes via a border collision bifurcation (see Fig. 4). The newly born equilibria are stable. By further increasing the parameter value $\mu_{BC} < \mu$, the origin loses stability at $\mu = \mu_{SN}$ by a saddle–node bifurcation in a two-dimensional subspace. For larger parameter values $\mu_{SN} < \mu$, the equilibria E^\pm lose their stability at $\mu = \mu_{RB}$ through a complex eigenvalue pair crossing the imaginary axis in doing so creating a stable limit cycle in what is called a rapid bifurcation [9,17]. To summarize, the bifurcation parameters are related as:

$$0 < \mu_{BC} < \mu_{SN} < \mu_{RB}. \tag{32}$$

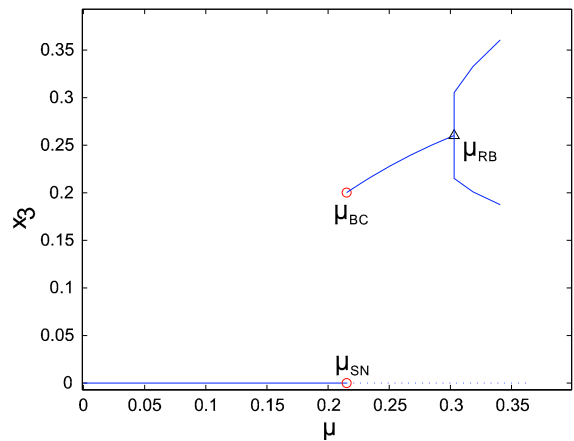


Fig. 6 Pitch-DOF bifurcation diagram

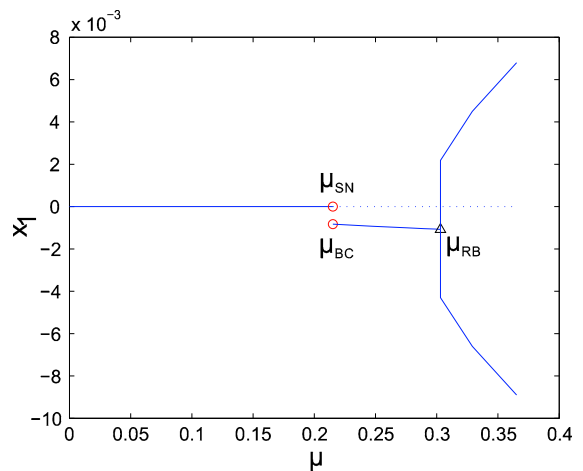


Fig. 7 Plunge-DOF bifurcation diagram

The bifurcation diagrams for the pitch and plunge DOF are generated numerically utilizing MATCONT [6], as shown in Figs. 6 and 7.

Roberts et al. [30] also use a numerical continuation method to dynamic piecewise aeroelastic systems. Thota and Dankowicz developed a toolbox (TC-HAT) for continuation of periodic orbits in hybrid dynamical systems [36].

4 Numerical results

Numerical simulations for the bilinear system dynamics are presented here (a more complete set of results is presented in [8]). The phase portraits of the pitch DOF in the (x_3, x_4) plane are presented for μ_1, μ_2, μ_3 and μ_4 , where

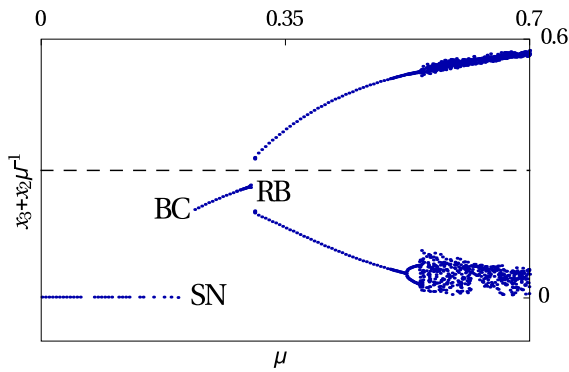


Fig. 8 Bifurcation diagram (*BC* border collision bifurcation, *SN* saddle–node bifurcation, *RB* rapid bifurcation)

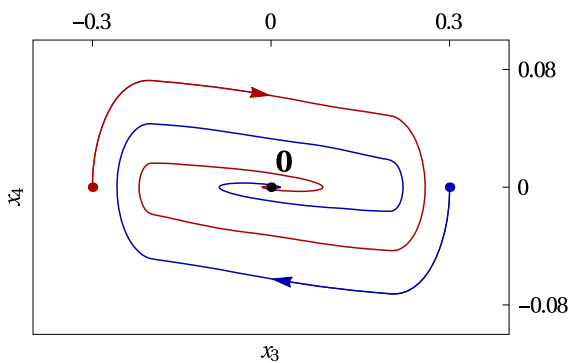


Fig. 9 Projection of typical trajectories for $\mu = \mu_1$, the origin is a stable equilibrium

$$0 < \mu_1 < \mu_{BC} < \mu_2 < \mu_{SN} < \mu_3 < \mu_{RB} < \mu_4. \tag{33}$$

In particular

$$\begin{aligned} \mu_1 &= 0.99\mu_{BC} = 0.2138, \\ \mu_2 &= 1.001\mu_{BC} = 0.999\mu_{SN} = 0.215, \\ \mu_3 &= 1.2\mu_{SN} = 0.85\mu_{RB} = 0.2583, \\ \mu_4 &= 1.04\mu_{RB} = 0.316. \end{aligned}$$

The bifurcation diagram (generated with Mathematica) in Fig. 8 is the intersection of the attractor and the hyperplane:

$$\{x \in \mathbb{R}^4 : x_4 = 0 \wedge x_3 > 0\}$$

projected onto x_3 for the parameter range $0 < \mu < 0.7$.

The first three bifurcations that the system undergoes are shown in Fig. 8. Figures 9 and 10 show typical trajectories of the system before ($\mu = \mu_1$) and after

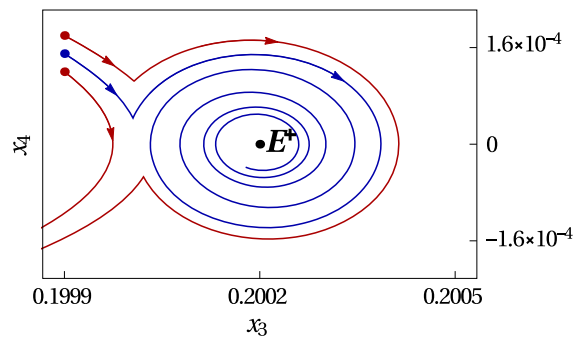


Fig. 10 Projection of trajectories near the equilibria E^+ after the border collision bifurcation for $\mu = \mu_2$

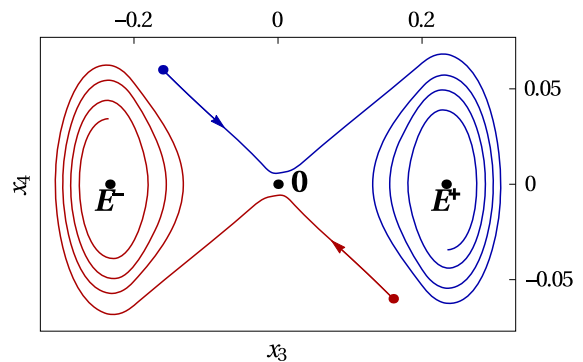


Fig. 11 Projection of two converging trajectories after the saddle–node bifurcation for $\mu = \mu_3$

the border collision bifurcation ($\mu = \mu_2$), respectively. Before the bifurcation, the only equilibrium is $\mathbf{0}$. Figure 11 shows that after the border collision bifurcation there are three equilibria, $\mathbf{0}$ and E^\pm . The equilibria E^\pm are stable for $\mu_{BC} \leq \mu < \mu_{RB}$.

Figures 9 and 11 illustrate the saddle–node bifurcation: before the bifurcation ($\mu = \mu_2$), trajectories converge toward $\mathbf{0}$, while after the bifurcation ($\mu = \mu_3$) the trajectories diverge from $\mathbf{0}$ and converge to one of the equilibria E^\pm . Figures 11 and 12 show trajectories before ($\mu = \mu_3$) and after ($\mu = \mu_4$) the rapid bifurcation. Before this bifurcation, the equilibria E^\pm are stable, and after the bifurcation they become unstable and limit cycles are born (Fig. 13).

Chaotic behavior is also observed in the bilinear model dynamics (see Fig. 14). The time history in Fig. 15 displays intermittent behavior [14]. This behavior has been observed in many experiments in [15], [40] and [13]. Alighanbari and Hashemi [2] also performed bifurcation analysis of an airfoil with a structural nonlinearity in the pitch direction. They observed

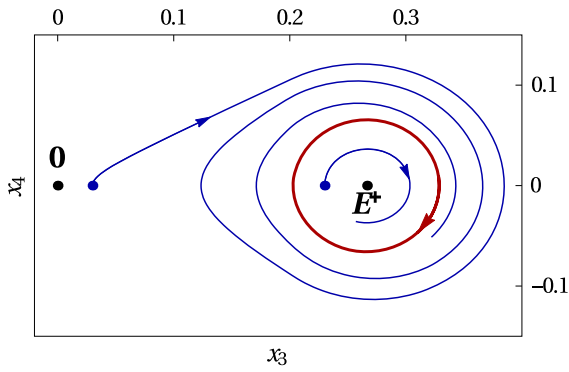


Fig. 12 Projection of a limit cycle and two converging trajectories after the rapid bifurcation for $\mu = \mu_4$

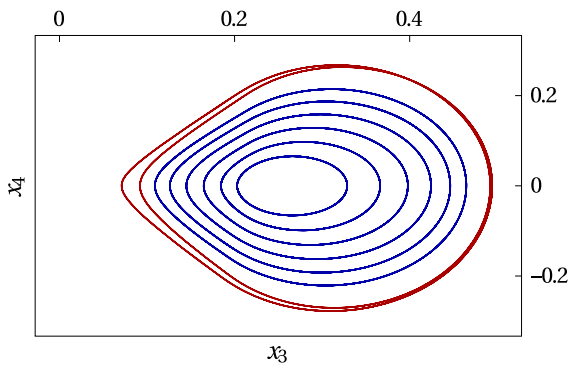


Fig. 13 After the rapid bifurcation, the amplitude of the limit cycle oscillation is increasing with μ , and then it undergoes a period doubling (the outermost limit cycle)

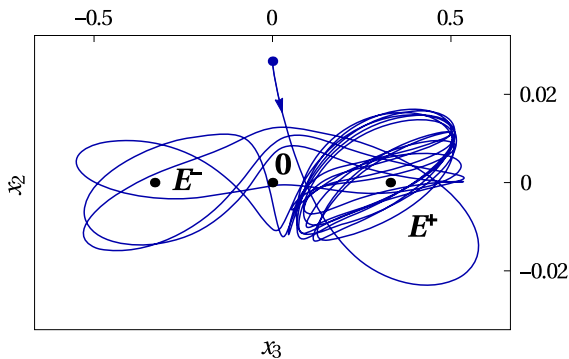


Fig. 14 Intermittent chaotic behavior for $\mu = 0.55$

the period doubling route to chaos in addition to a mildly chaotic behavior in a narrow range of the bifurcation parameter. Period doubling is observed in our case as well (see Fig. 13).

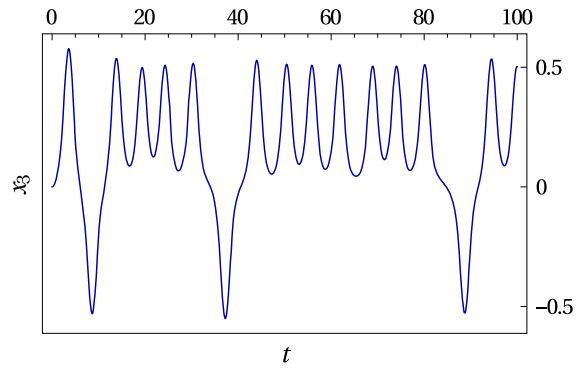


Fig. 15 Intermittent chaotic behavior for $\mu = 0.55$

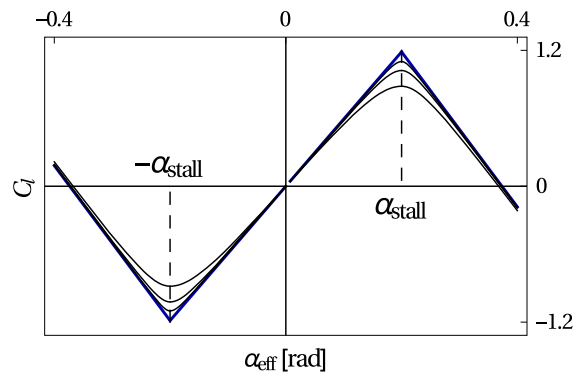


Fig. 16 Bilinear model and its approximation by a family of continuously differentiable functions

5 Model validity and robustness

The bilinear model and the original piecewise linear system are equivalent when $|\alpha_{\text{eff}}| \leq \alpha_{\text{switch}}$. The saddle-node and border collision bifurcations also occur in the original system. When the rapid bifurcation occurs, the newly born limit cycle lies outside of the equivalency domain (above the dashed line in Fig. 8).

To examine the robustness of the model, we modify the bilinear function to provide a smoother transition between the pre-stall and post-stall regimes. We look at the function $x \mapsto |x|$ as the limit of the hyperboles $x \mapsto \sqrt{x^2 + \epsilon^2}$ when $\epsilon \rightarrow 0$.

Using this idea, we constructed a family of maps (Fig. 16) parametrized by $\epsilon > 0$:

$$C_l(\alpha_{\text{eff}}, \epsilon) = \begin{cases} C_{l1}(\alpha_{\text{eff}}, \epsilon) & |\alpha_{\text{eff}}| \leq \alpha_{\text{stall}} \\ C_{l2}(\alpha_{\text{eff}}, \epsilon) & \alpha_{\text{stall}} \leq |\alpha_{\text{eff}}|, \end{cases} \quad (34)$$

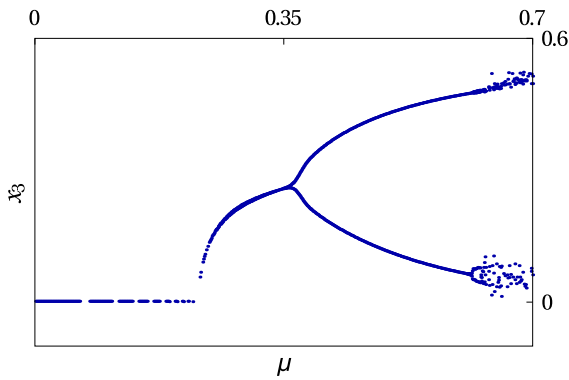


Fig. 17 Bifurcation diagram for the smooth system with parameter value $\epsilon = 0.1$

where

$$C_{l1}(\alpha_{\text{eff}}, \epsilon) = -c_0 \operatorname{sgn}(\alpha_{\text{eff}}) \left(\sqrt{(|\alpha_{\text{eff}}| - \alpha_{\text{stall}})^2 + \epsilon^2} - \sqrt{\alpha_{\text{stall}}^2 + \epsilon^2} \right), \tag{35}$$

$$C_{l2}(\alpha_{\text{eff}}, \epsilon) = \operatorname{sgn}(\alpha_{\text{eff}}) \left(c_1 \sqrt{(|\alpha_{\text{eff}}| - \alpha_{\text{stall}})^2 + \eta^2(\epsilon)} + c_0 \alpha_{\text{stall}} \right), \tag{36}$$

where

$$\eta(\epsilon) = \frac{c_0}{c_1} \left(\alpha_{\text{stall}} + \epsilon - \sqrt{\alpha_{\text{stall}}^2 + \epsilon^2} \right).$$

Note that $C_l(\alpha_{\text{eff}}, \epsilon)$ is in the class of continuously differentiable functions, thus providing a smoother transition between the two regimes, while in the limit the original bilinear function is recovered: $C_l(\alpha_{\text{eff}}) = \lim_{\epsilon \rightarrow 0^+} C_l(\alpha_{\text{eff}}, \epsilon)$. Every member of this family has the same asymptotics as the bilinear function, that is

$$\lim_{|\alpha_{\text{eff}}| \rightarrow \infty} |C_l(\alpha_{\text{eff}}, \epsilon) - C_l(\alpha_{\text{eff}})| = 0,$$

furthermore $C_l(0, \epsilon) = C_l(0) = 0$. Substituting this into Eq. (9), we obtain a smooth system instead of a piecewise linear one. A bifurcation diagram for the smooth system ($\epsilon = 0.1$) is shown in Fig. 17.

It can be seen that the border collision bifurcation is disappeared, because there is no actual border but a smooth transition between the regimes. The rapid bifurcation is also gone; instead, there is a Hopf bifurcation occurring. A chaotic region is also present in the smooth system. Nonetheless, the bifurcation diagrams

of the bilinear system retain the same features. Thus, we deem the bilinear system a good approximation of the smooth system.

6 Discussion and conclusion

Nonlinear analysis of aeroelastic systems is a topic that has been widely covered in the literature. The nonlinearities in aeroelastic systems can be aerodynamic and/or structural nonlinearities. Many models were introduced to address these nonlinearities and study their effects on aeroelastic systems. In this paper, aerodynamic nonlinearities arising from the stall behavior of an aeroelastic system were studied on a 2-DOF (pitch and plunge) model. A piecewise linear model utilizing experimental data for the lift coefficient versus the angle of attack for a NACA 0012 airfoil was proposed.

The equations of motion for the system were nondimensionalized. The nondimensional freestream velocity was introduced as the system bifurcation parameter.

A simplified bilinear model was then extracted from the full piecewise linear model and analyzed. Equilibrium points of the bilinear model were found analytically as a function of the bifurcation parameter. Stability criteria of those equilibrium points were then established by applying the Liénard–Chipart theorem. Bifurcation diagrams of the system were calculated utilizing MATCONT and Mathematica.

The analysis found bifurcations that are intrinsic to piecewise systems such as border collision and the rapid bifurcations. The border collision bifurcation describes the sudden birth of equilibria E^\pm , and the rapid bifurcation explains the creation of a finite-amplitude stable limit cycle. Chaotic behavior was also found, and the intermittent route to chaos was observed numerically.

To better understand the underlying dynamical behavior, one needs to pinpoint the mechanism leading to the sensitivity on initial conditions. It is now widely accepted that grazing (just-touching behavior of trajectories) is directly responsible for complex behavior (see, for example, Bernardo et al. [5]). The decomposition of the state space into domains separated by switching planes paves the way to the description of the system behavior by symbolic dynamics. In particular, the system behavior can be characterized by the evolution of sets of initial conditions lying on the switching planes Σ^\pm . A symbolic dynamics based analysis will be the subject of a follow-up paper.

Finally, it is important to highlight that some of the results presented in this work exceed the boundaries of the physical validity of the model for an airfoil. The analysis was conducted on the bilinear model assuming no restrictions on the range of the angle of attack. The chaotic behavior observed can be attributed to the model being beyond the valid range.

Acknowledgments The authors are grateful to the reviewers whose suggestions helped to improve the paper. This research was partially supported by OTKA-84060. This research was partially supported by the Hungarian Scientific Research Fund OTKA-84060.

References

- Abdelkefi, A., Vasconcellos, R., Nayfeh, A.H., Hajj, M.R.: An analytical and experimental investigation into limit-cycle oscillations of an aeroelastic system. *Nonlinear Dyn.* **71**(1–2), 159–173 (2013)
- Alighanbari, H., Hashemi, S.: Derivation of odes and bifurcation analysis of a two-dof airfoil subjected to unsteady incompressible flow. *Int. J. Aerosp. Eng.* (2009)
- Andronov, A.A., Vitt, A.A., Khaikin, S.E.: *Theory of Oscillators*. Pergamon Press Ltd, New York (1966)
- Antali, M., Stepan, G.: Discontinuity-induced bifurcations of a dual-point contact ball. *Nonlinear Dyn.* pp. 1–18 (2015)
- Bernardo, M., Budd, C.J., Champneys, A.R., Kowalczyk, P.: *Piecewise-Smooth Dynamical Systems: Theory and Applications*, vol. 2. Springer, London (2008)
- Dhooge, A., Govaerts, W., Kuznetsov, Y.A.: MATCONT: a matlab package for numerical bifurcation analysis of ODEs. *ACM Trans. Math. Softw.* **29**, 141–164 (2003)
- Dowell, E., Edwards, J., Strganac, T.W.: Nonlinear aeroelasticity. *J. Aircr.* **40**(5), 857–874 (2003)
- Elgohary, T.: *Nonlinear Analysis of a Two DOF Piecewise Linear Aeroelastic System*. Master's thesis, Texas A&M University (2010)
- Freire, E., Ponce, E., Ros, J.: Limit cycle bifurcation from center in symmetric piecewise-linear systems. *Int. J. Bifurcation Chaos* **9**(5), 895–907 (1999)
- Gantmacher, F.R.: *The Theory of Matrices*, vol. 2. Chelsea Publishing Company, New York (1959)
- Gilliatt, H.C., Strganac, T.W., Kurdila, A.J.: Nonlinear aeroelastic response of an airfoil. In: *Proceedings of the 35th Aerospace Sciences Meeting and Exhibit*. AIAA 97-459, Reno, NV (1997)
- Gilliatt, H.C., Strganac, T.W., Kurdila, A.J.: An investigation of internal resonance in aeroelastic systems. *Nonlinear Dyn.* **31**, 1–22 (2003)
- Hayashi, H., Ishizuka, S., Hirakawa, K.: Transition to chaos via intermittency in the onchidium pacemaker neuron. *Phys. Lett. A* **98**(8–9), 474–476 (1983)
- Hilborn, R.C.: *Chaos and Nonlinear Dynamics : An Introduction for Scientists and Engineers*. Oxford University Press, Oxford (2000)
- Jeffries, C., Perez, J.: Observation of a pomeau-manneville intermittent route to chaos in a nonlinear oscillator. *Phys. Rev. A* **26**(4), 2117–2122 (1982)
- Kalmár-Nagy, T., Wahi, P., Halder, A.: Dynamics of a hysteretic relay oscillator with periodic forcing. *SIAM J. Appl. Dyn. Syst.* **10**, 403–422 (2011)
- Kriegsmann, G.: The rapid bifurcation of the Wien bridge oscillator. *IEEE Trans. Circuits Syst.* **34**(9), 1093–1096 (1987)
- Lee, B.H.K., Price, S.J., Wong, Y.S.: Nonlinear aeroelastic analysis of airfoils: bifurcation and chaos. *Prog. Aerosp. Sci.* **35**(3), 205–334 (1999)
- Leine, R.I.: Bifurcations of equilibria in non-smooth continuous systems. *Phys. D-Nonlinear Phenom.* **223**, 121–137 (2006)
- Llibre, J., Novaes, D.D., Teixeira, M.A.: Maximum number of limit cycles for certain piecewise linear dynamical systems. *Nonlinear Dyn.* **82**(3), 1159–1175 (2015)
- Magri, L., Galvanetto, U.: Example of a non-smooth hopf bifurcation in an aero-elastic system. *Mech. Res. Commun.* **40**, 26–33 (2012)
- Mahfouz, I.A., Badrakhhan, F.: Chaotic behavior of some piecewise-linear systems. I. Systems with set-up spring or with unsymmetric elasticity. *J. Sound Vib.* **143**, 255–288 (1990)
- Mahfouz, I.A., Badrakhhan, F.: Chaotic behavior of some piecewise-linear systems. 2. Systems with clearance. *J. Sound Vib.* **143**, 289–328 (1990)
- Makarenkov, O., Lamb, J.S.: Dynamics and bifurcations of nonsmooth systems: a survey. *Phys. D* **241**(22), 1826–1844 (2012)
- O'Neil, T., Gilliatt, H.C., Strganac, T.W.: Investigations of aeroelastic response for a system with continuous structural nonlinearities. In: *Proceedings of the 37th Structures, Structural Dynamics and Materials Conference*. AIAA 96-1390, Salt Lake City, UT (1996)
- O'Neil, T., Strganac, T.W.: Aeroelastic response of a rigid wing supported by nonlinear springs. *J. Aircr.* **35**, 616–622 (1998)
- Pratap, R., Mukherjee, S., Moon, F.C.: Dynamic behavior of a bilinear hysteretic elastoplastic oscillator 1. Free oscillations. *J. Sound Vib.* **172**, 321–337 (1994)
- Pratap, R., Mukherjee, S., Moon, F.C.: Dynamic behavior of a bilinear hysteretic elastoplastic oscillator. 2. Oscillations under periodic impulse forcing. *J. Sound Vib.* **172**, 339–358 (1994)
- Price, S.J., Alighanbari, H., Lee, B.H.K.: The aeroelastic response of a 2-dimensional airfoil with bilinear and cubic structural nonlinearities. *J. Fluids Struct.* **9**, 175–193 (1995)
- Roberts, I., Jones, D., Lieven, N., Di Bernardo, M., Champneys, A.: Analysis of piecewise linear aeroelastic systems using numerical continuation. *Proc. Inst. Mech. Eng. Part G: J. Aerosp. Eng.* **216**(1), 1–11 (2002)
- Seiranyan, A.P.: Collision of eigenvalues in linear oscillatory systems. *J. Appl. Math. Mech.* **58**, 805–813 (1994)
- Shaw, S.W., Holmes, P.J.: A periodically forced piecewise linear-oscillator. *J. Sound Vib.* **90**, 129–155 (1983)
- Sheldahl, R.E., Klimas, P.C.: Aerodynamic characteristics of seven symmetrical airfoil sections through 180-degree angle of attack for use in aerodynamic analysis of vertical

- axis wind turbines. Tech. rep., Sandia National Laboratories. SAND80-2114 (1981)
34. Tang, D.M., Dowell, E.H.: Flutter and stall response of a helicopter blade with structural nonlinearity. *J. Aircr.* **29**, 953–960 (1992)
 35. Tang, D.M., Dowell, E.H.: Comparison of theory and experiment for nonlinear flutter and stall response of a helicopter blade. *J. Sound Vib.* **165**, 953–960 (1993)
 36. Thota, P., Dankowicz, H.: Tc-hat (tc): a novel toolbox for the continuation of periodic trajectories in hybrid dynamical systems. *SIAM J. Appl. Dyn. Syst.* **7**(4), 1283–1322 (2008)
 37. Ueda, T., Dowell, E.H.: Flutter analysis using nonlinear aerodynamic forces. *J. Aircr.* **21**, 101–109 (1984)
 38. Vieth, E.: Fitting piecewise linear regression functions to biological responses. *J. Appl. Physiol.* **67**(1), 390–396 (1989)
 39. Woolston, D.S., Runyan, H.L., Andrews, R.E.: An investigation of effects of certain types of structural nonlinearities on wing and control surface flutter. *J. Aeronaut. Sci.* **24**, 57–63 (1957)
 40. Yeh, W.J., Kao, Y.H.: Universal scaling and chaotic behavior of a josephson-junction analog. *Phys. Rev. Lett.* **49**(26), 1888–1891 (1982)
 41. Zhusubaliyev, Z.T., Mosekilde, E.: *Bifurcations and Chaos in Piecewise-Smooth Dynamical Systems*. World Scientific, River Edge (2003)